Supplementary Information

Room-temperature synthesis of nonstoichiometric copper sulfide ($Cu_{2-x}S$) for sodium ion storage

Zhiwen Tang,[a] Yuede Pan,*[ab] Qianrui Zhao,[a] Yiming Cao,[a] Chenying Su,[a] Peng Gao,*[c] Zonghang Liu,[d] Yanxia Chen,[e] Gang Li,*[a] Qin Wang,[a] Zhewei Yang,[a] Chunli Guo[a] and Kaiying Wang[a]

[a] Institute of Energy Innovation, College of Materials Science and Engineering, Taiyuan University of Technology, Taiyuan 030024, China.

[b] Key Laboratory of Advanced Energy Materials Chemistry (Ministry of Education), College of Chemistry, Nankai University, Tianjin 300071, China

[c] School of Chemistry and Molecular Bioscience, University of Wollongong, NSW 2500, Australia.

[d] School of Science and Engineering, Shenzhen Key Laboratory of Functional Aggregate Materials, The Chinese University of Hong Kong, Shenzhen 518172, China.

[e] Beijing Key Laboratory for Sensor, Beijing Information Science and Technology University, Beijing 100101, China

*Corresponding authors:
panyuede@tyut.edu.cn (Y. Pan);
penggao2022@gmail.com (P. Gao);
ligang02@tyut.edu.cn (G. Li)

1 Experimental section

1.1 Material synthesis

$CuCl_2 \cdot 2H_2O$ (Analytical Reagent, Aladdin Scientific Corp.) and $Na_2S \cdot 9H_2O$ (99.99%, Aladdin Scientific Corp.) were used as received. Typically, the aqueous solution of $CuCl_2$ (0.5 M, 10 ml) was added with the aqueous solution of sodium sulfide (0.5 M, 100 ml) for the preparation of $Cu_{2-x}S$. For comparison, another four samples were obtained by adding 12, 24, 36, 48 and 200 ml of the aqueous solution of sodium sulfide (0.5 M), respectively. The mixed solutions were stirred for 3 h before the solid products were collected, washed with deionized water and ethanol, and dried.

1.2 Characterizations

Morphologies were observed using a ZEISS Geimini 300 field emission scanning electron microscope (SEM, 2.00 kV) and a JEM-2100F Transmission electron microscope (TEM). High-resolution TEM (HRTEM) and selected area electron diffraction (SAED) images were also collected using the JEM-2100F TEM. The phase composition was identified using Cu Kα radiation (λ=0.154059 nm) on SmartLab SE03030502-X-ray diffractometer (XRD, RIGATONI CORPORATION, Japan). The Rietveld analysis of XRD data was carried out using GSAS-II. Raman spectra were collected on a Raman spectrometer (Invia Reflex, Renishaw, U.K). The X-ray photoelectron spectra were obtained on an XPS instrument (Escalab 250Xi, Thermo Fisher, USA). The optical absorption spectra were acquired with a thermostatic quartz cell (1 cm) in the wavelength range of 200–800 nm using an UV-5000 Plus spectrophotometer (Agilent, America).

1.3 Electrochemical Measurements

The active material, Super P and polyvinylidene fluoride (PVDF) were mixed in a weight ratio 75:10:15 with the addition of N-methylpyrrolidone (NMP) and grounded to form a homogeneous slurry, which was then coated on copper foil and dried in

vacuum at 80 °C. The active material loading of the electrode was around 1 mg cm^{-2}. The as-prepared electrode was cut into circular pieces with a diameter of 12 mm for use.

Cell assembly was carried out in a glove box filled with argon (H_2O < 0.1 ppm, O_2 < 0.1 ppm). The as-prepared electrode was assembled into coin cells with Na foil as the anode; the electrolytes was 1.0 M $NaCF_3SO_3$ in diethylene glycol dimethyl ether (DEGDME). The cells were charged and discharged in the range of 0.3-3 V on a Neware battery tester. Cyclic voltammetry (CV) curves were obtained on a CHI1030C electrochemical workstation.

1.4 Theoretical calculation methods

To understand the Na^+ diffusion in CuS and $Cu_{2-x}S$ structures, CINEB methods were used. The diffusion ability has been described by energy barrier. DFT calculations were performed using the GGA+U sheme[1] with projector augmented wave (PAW) method[2] as executed in the Vienna ab initio simulation package (VASP)[3]. Exchange-correlation effects were included using Perdew-Burke-Ernzerhof (PBE)[4] and the U term was set as 5 eV for Cu 3d orbit[5]. In geometric optimization and NEB[5] phase, a 5×5×5 and 5×2×5 k-mesh was used for Brillouin zone (BZ) sampling in Cu_2S/CuS system with an energy cutoff of 500 eV. To prove lattice dynamics stability, the phonon approach was employed using the Phonopy package[6]. The electronic convergence was setting of 1×10^{-9} eV. For local Na-ion migration analysis, the climbing-image nudged elastic band (CINEB) methods[7] were used. For each initial and final state configuration of the Na^+ jump, the total of 5 intermediate images were created for CuS and Cu_2S (V_{Cu}) transport system, respectively. Cu_2S is a cubic crystal (space group FM-3M) at room temperature and the lattice constants of a=b=c=5.503 Å (in experiment) or a=b=5.613 Å and c=5.5032 Å (in simulation).

References

1 Rohrbach, A., Hafner, J., Kresse, G. Electronic correlation effects in transition-metal

sulfides. *J. Phys. Condens. Matter.*, 2003, **15,** 979-996.

2 Blochl, P. E. Projector Augmented-Wave Method. *Phys. Rev. B*, 1994, **50,** 17953-17979.

3 Kresse, G., Furthmuller, J. Efficient iterative schemes for ab initio total-energy calculations using a plane-wave basis set. *Phys. Rev. B*, 1996, **54,** 11169.

4 Perdew, J. P., Burke, K., Ernzerhof, M. Generalized gradient approximation made simple. *Phys. Rev. Lett.*, 1996, **77,** 3865.

5 Mikhlin, Y., Nasluzov, V., Ivaneeva, A., et al. Formation, evolution and characteristics of copper sulfide nanoparticles in the reactions of aqueous cupric and sulfide ions. *Mater. Chem. Phys.*, 2020, **255,** 123600.

6 Togo, A., Tanaka, I. First principles phonon calculations in materials science. *Scr. Mater.*, 2015, **108,** 1-5.

7 Henkelman, G., Uberuaga, B. P., Jonsson, H. A., A climbing image nudged elastic band method for finding saddle points and minimum energy paths. *J. Chem. Phys.*, 2000, **113,** 9901-9904.

2 Supplementary Figures

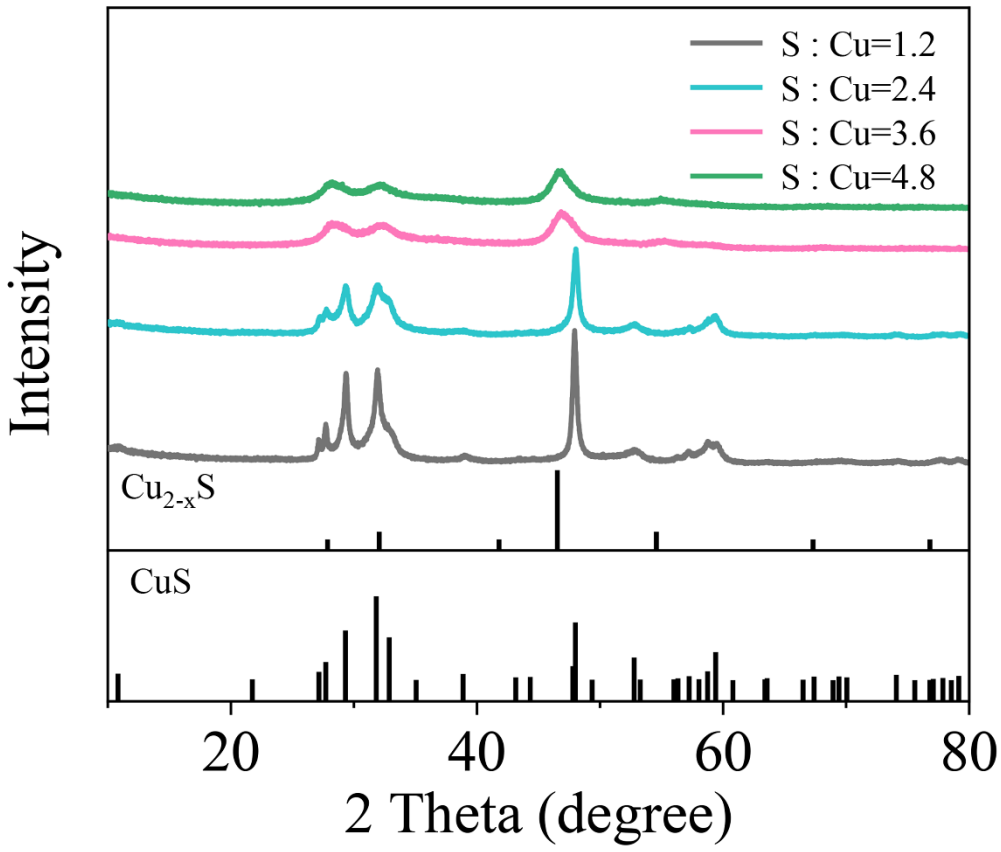

Figure S1. XRD patterns of the precipitates for the experiments with S/Cu = 1.2, 2.4, 3.6 and 4.8.

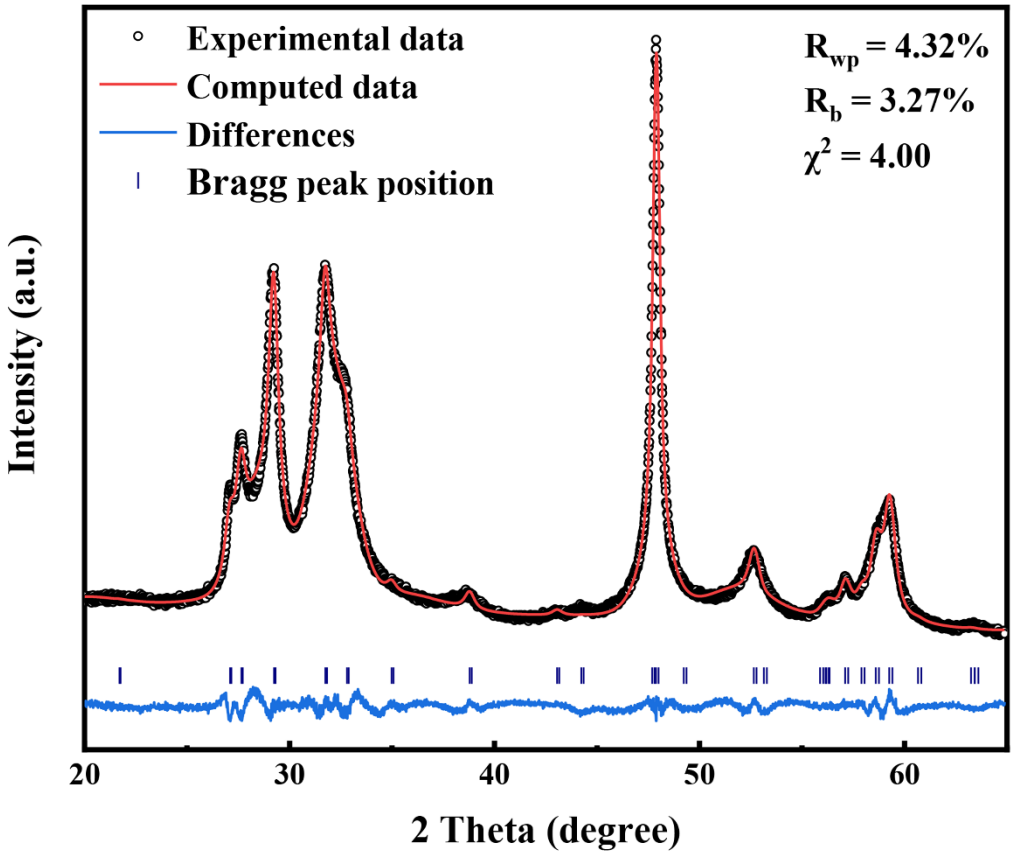

Figure S2. Rietveld refined XRD pattern of the precipitate for the S/Cu = 1.2 experiment with experimental data (black circles), calculated profiles (red line), allowed Bragg diffraction positions (vertical bars) and difference curve (blue line). All the peaks of the product could be assigned to the hexagonal CuS with the P63/mmc (no. 194) structure and lattice constants of a = b = 3.797 Å and c = 16.368 Å (JCPDS No. 01-079-2321). It consists of alternating disulfides (2/3) and monosulfides (1/3), as well as Cu atoms in tetrahedral (2/3) and triangular (1/3) coordination. The Rietveld analysis indicates 100% CuS with no impurities.

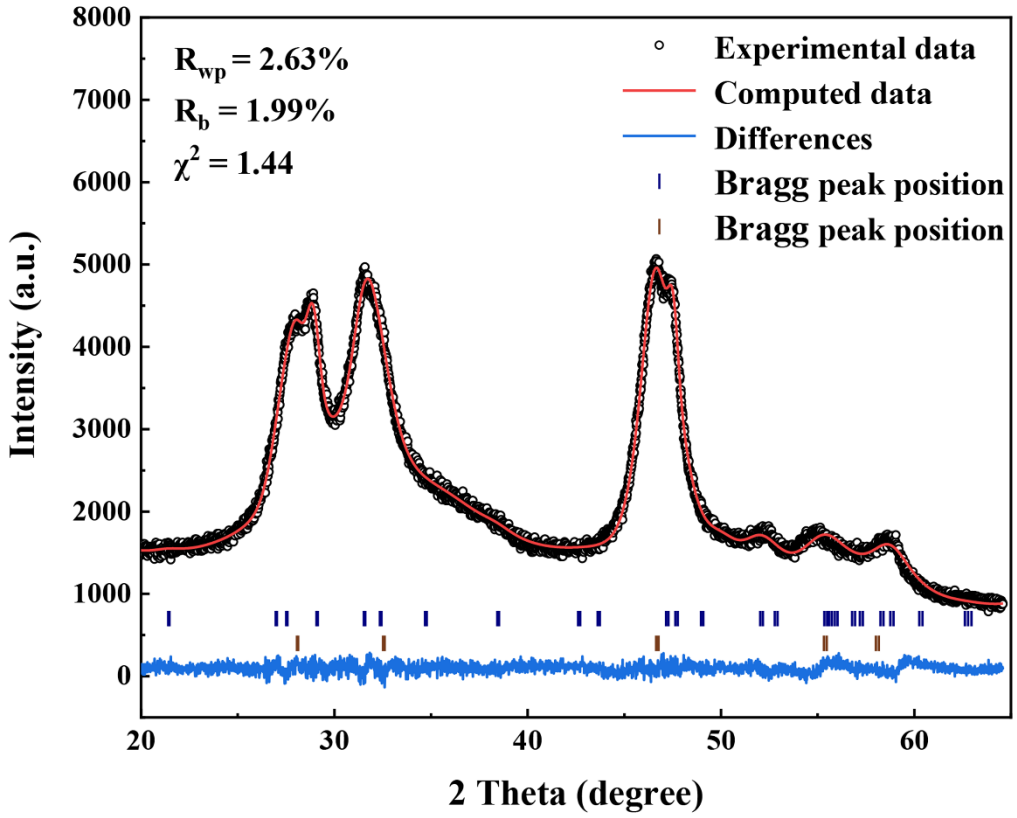

Figure S3. Rietveld refined XRD pattern of the precipitate for the S/Cu = 3.6 experiment with experimental data (black circles), calculated profiles (red line), allowed Bragg diffraction positions (vertical bars) and difference curve (blue line). The Rietveld analysis indicates a composite of $Cu_{2-x}S$/CuS (39.4: 60.6).

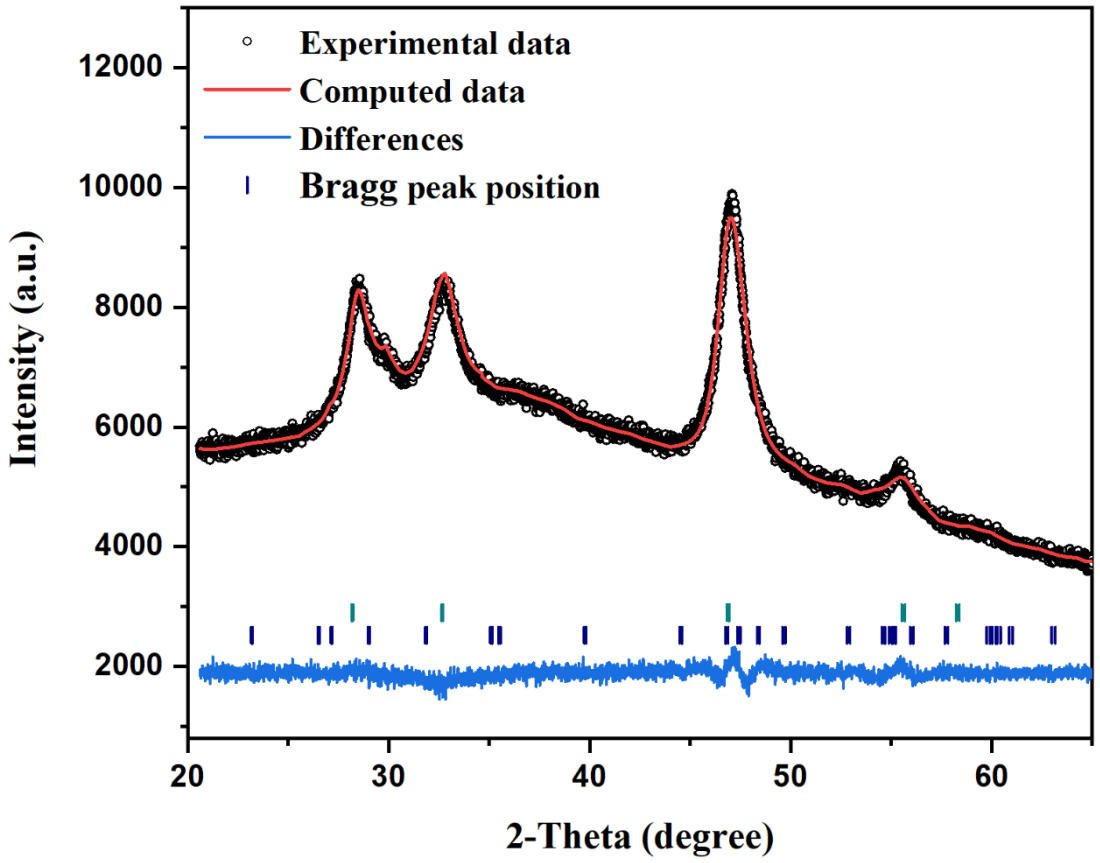

Figure S4. Rietveld refined XRD pattern of the precipitate for the S/Cu = 20 experiment with experimental data (black circles), calculated profiles (red line), allowed Bragg diffraction positions (vertical bars) and difference curve (blue line). The Rietveld analysis indicates a composite of $Cu_{2-x}S$/CuS (98.9: 1.1).

Table S1. Sample compositions for S/Cu = 1.2, 3.6, 10 and 20 experiments.

S/Cu ratio	1.2	3.6	10	20
$Cu_{2-x}S$ content (%)	0	39.4	98.8	98.9
CuS content (%)	100	60.6	1.2	1.1

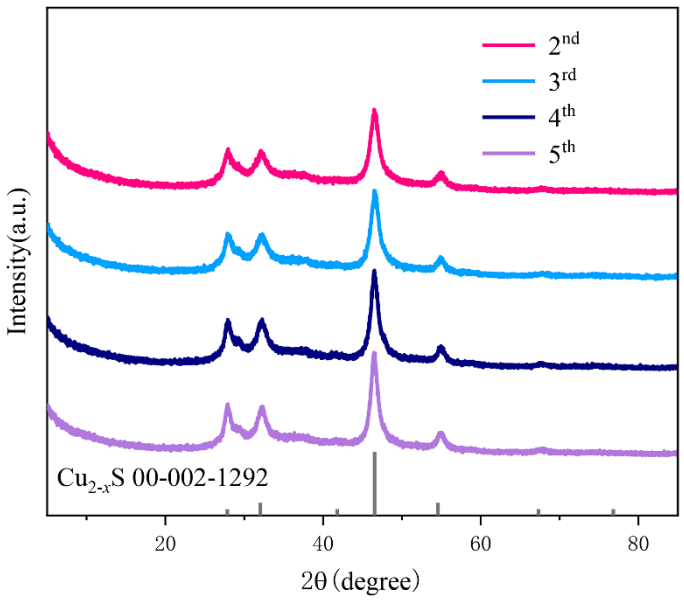

Figure S5. XRD patterns of the precipitates obtained after cyclic utilization of the supernatant for the S/Cu = 10 experiment. During the 5 cycles, the precipitates stay unchanged as $Cu_{2-x}S$.

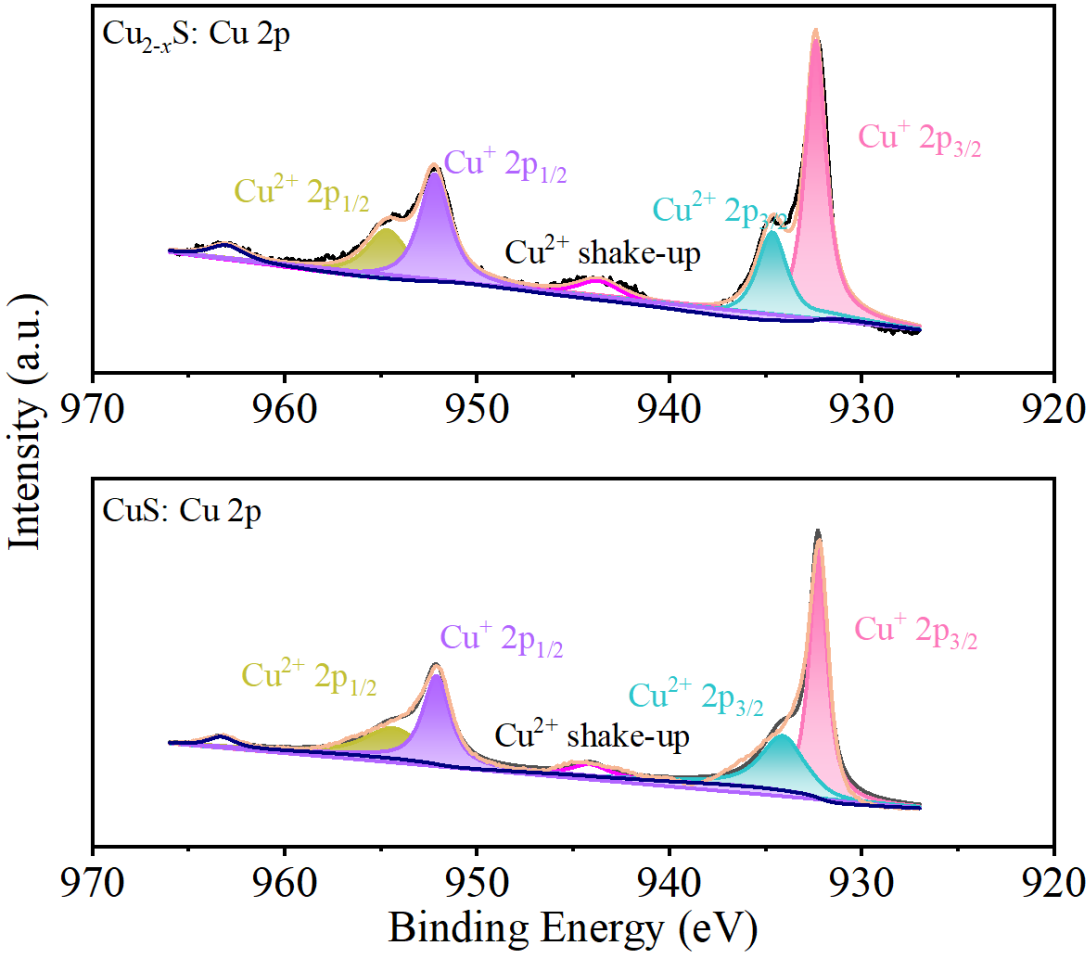

Figure S6. High-resolution XPS spectra of Cu 2p for $Cu_{2-x}S$ and CuS.

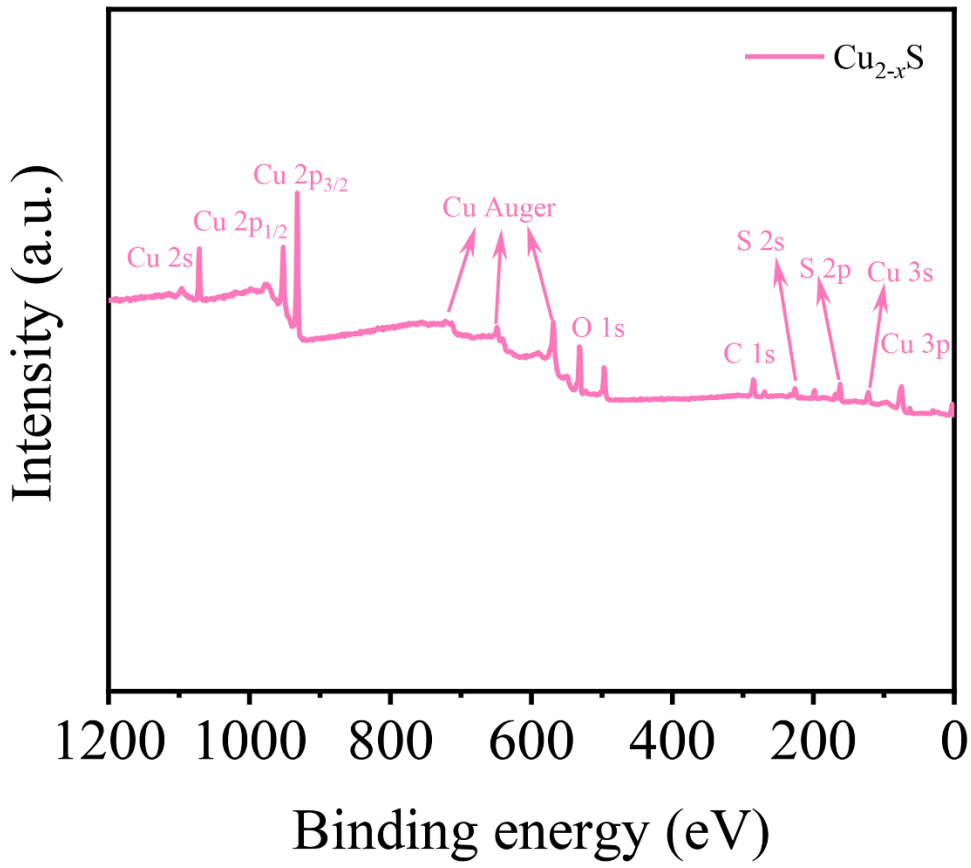

Figure S7. XPS survey spectrum of $Cu_{2-x}S$.

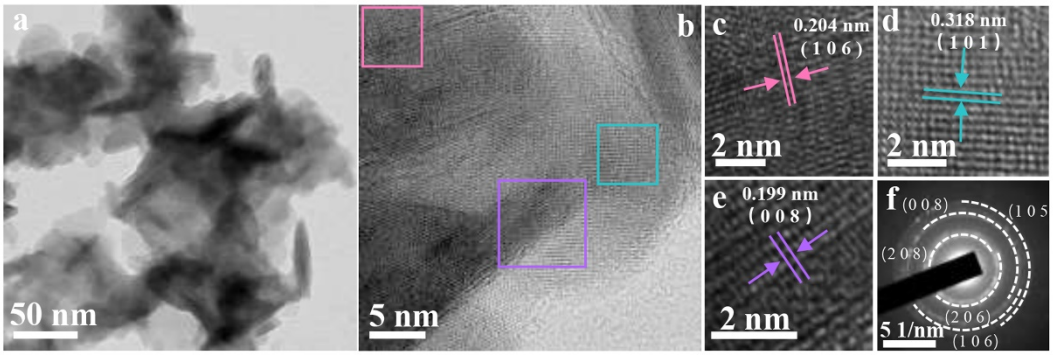

Figure S8. (a) TEM, (b-e) HRTEM, and (f) SAED images of CuS.

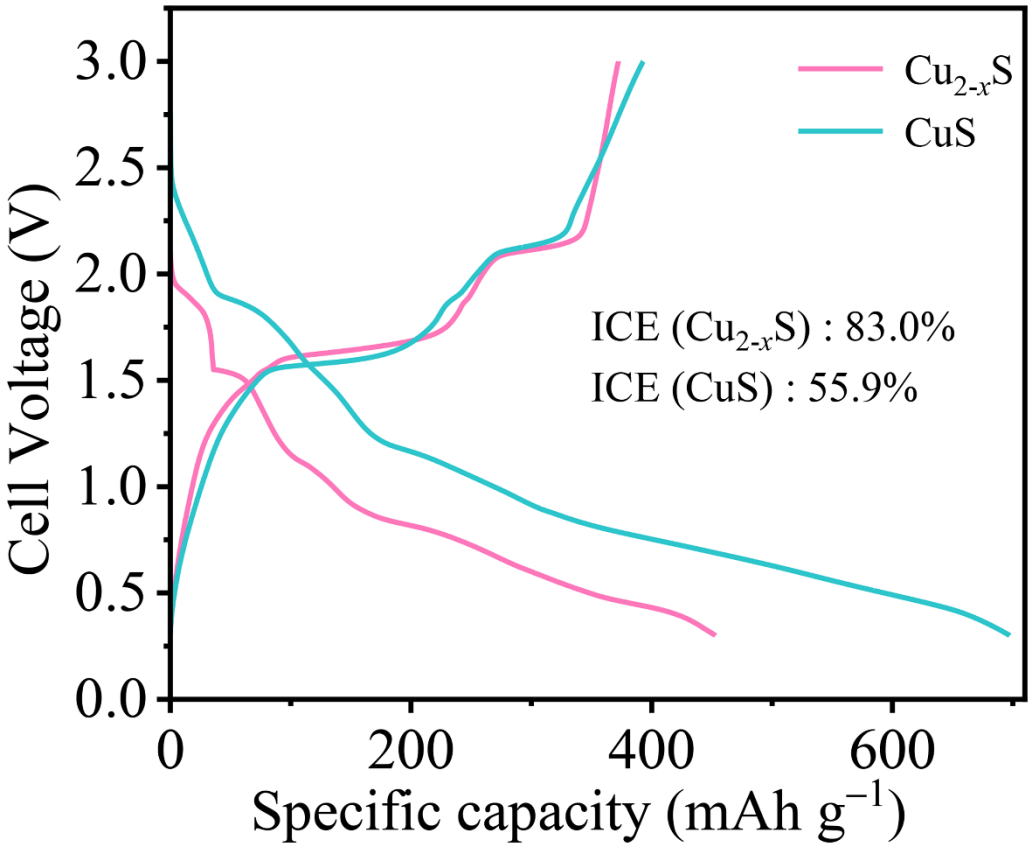

Figure S9. First-cycle GCD curves and the corresponding ICEs of $Cu_{2-x}S$ and CuS.

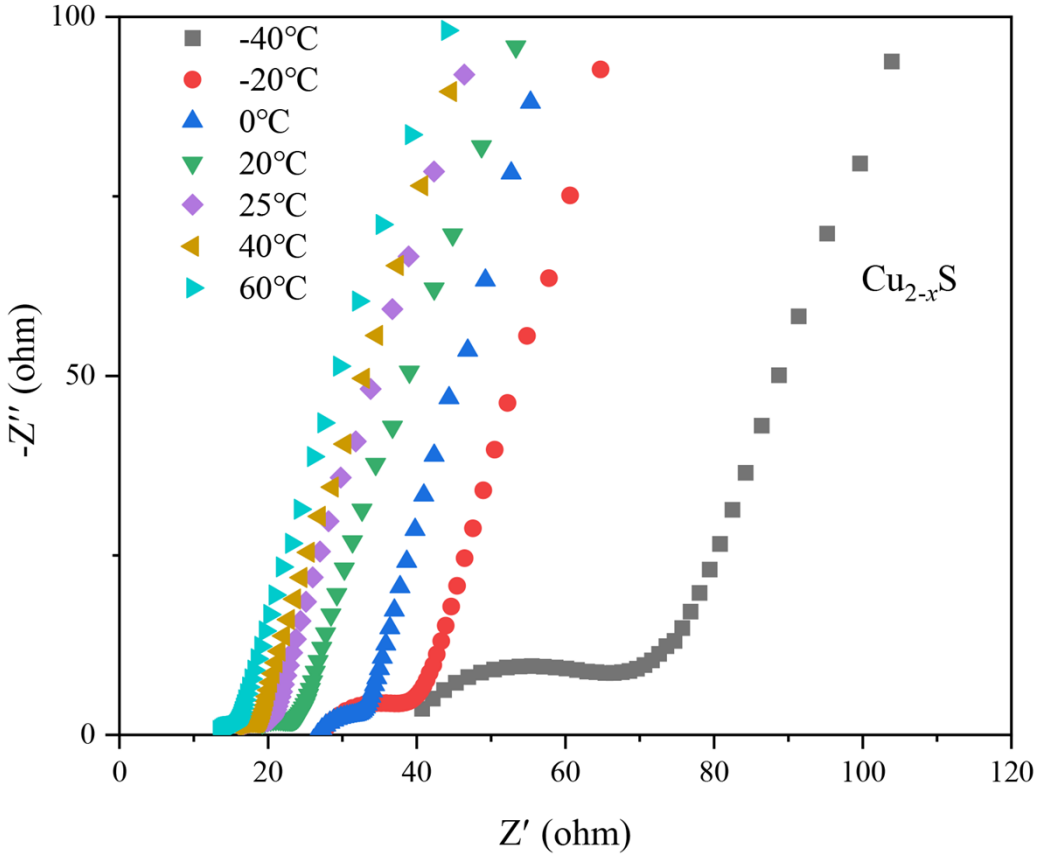

Figure S10. Nyquist plots for $Cu_{2-x}S$ at different temperatures.

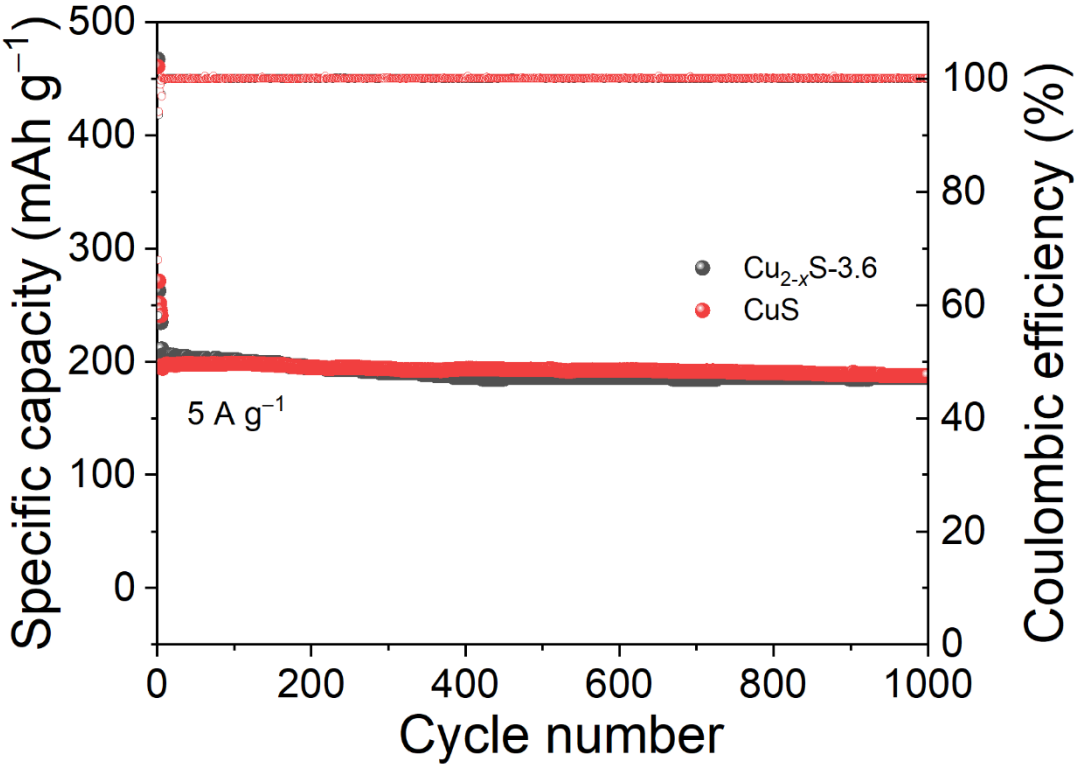

Figure S11. Cycling performance of CuS and $Cu_{2-x}S$-3.6 batteries.

Table S2. Sodium ion storage performance comparison between our work and those for copper oxide and other chalcogenides.

Anode material	Reversible capacity (mAh g^{-1}), cycle number	Current density (A g^{-1})	Ref
CuO	170, 100	0.1	*CrystEngComm*, 2021,23, 6107-6116
CuSe	285, 6000	10	*Electrochimica Acta*, 2022, 404, 139703
CuTe	290, n/a	n/a	*Applied Surface Science*, 2022, 573, 151550
CuS	187, 1000	5	*This work*
$Cu_{2-x}S$	288, 3000	2	*This work*
$Cu_{2-x}S$	237, 3000	5	*This work*

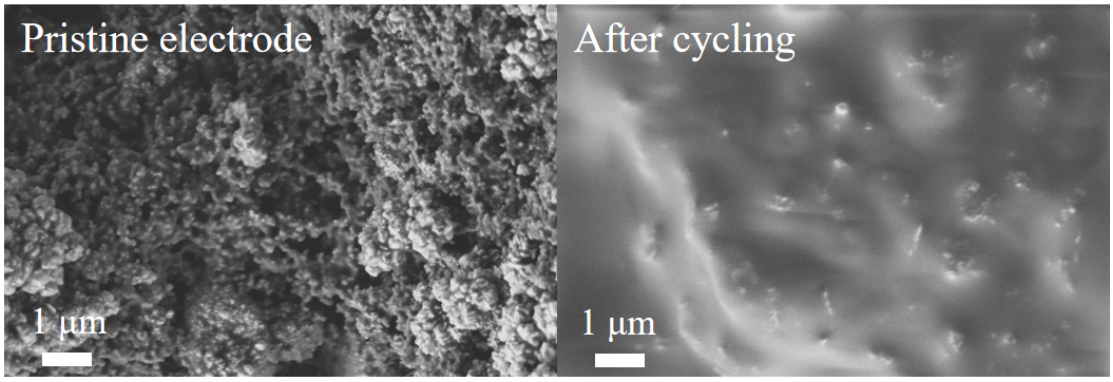

Figure S12. SEM images of the $Cu_{2-x}S$ electrode before and after cycling.

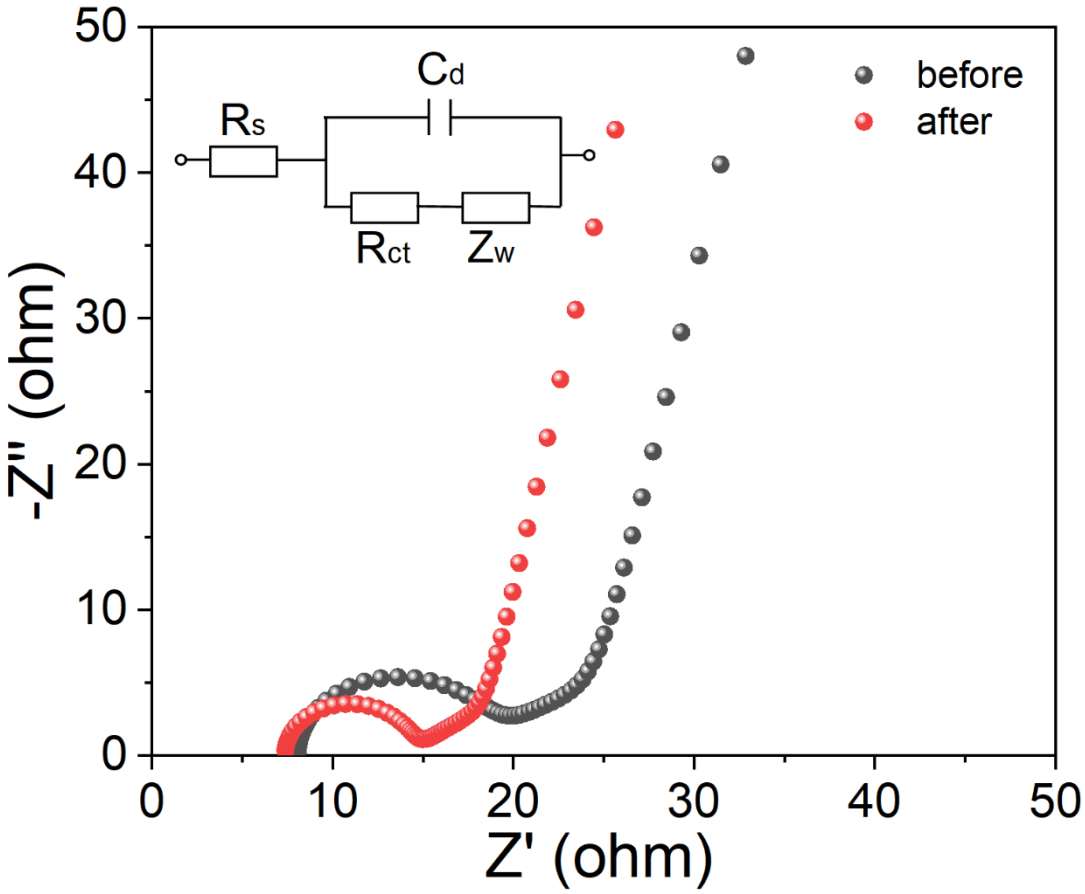

Figure S13. Nyquist plots of the $Cu_{2-x}S$ battery before and after cycling.

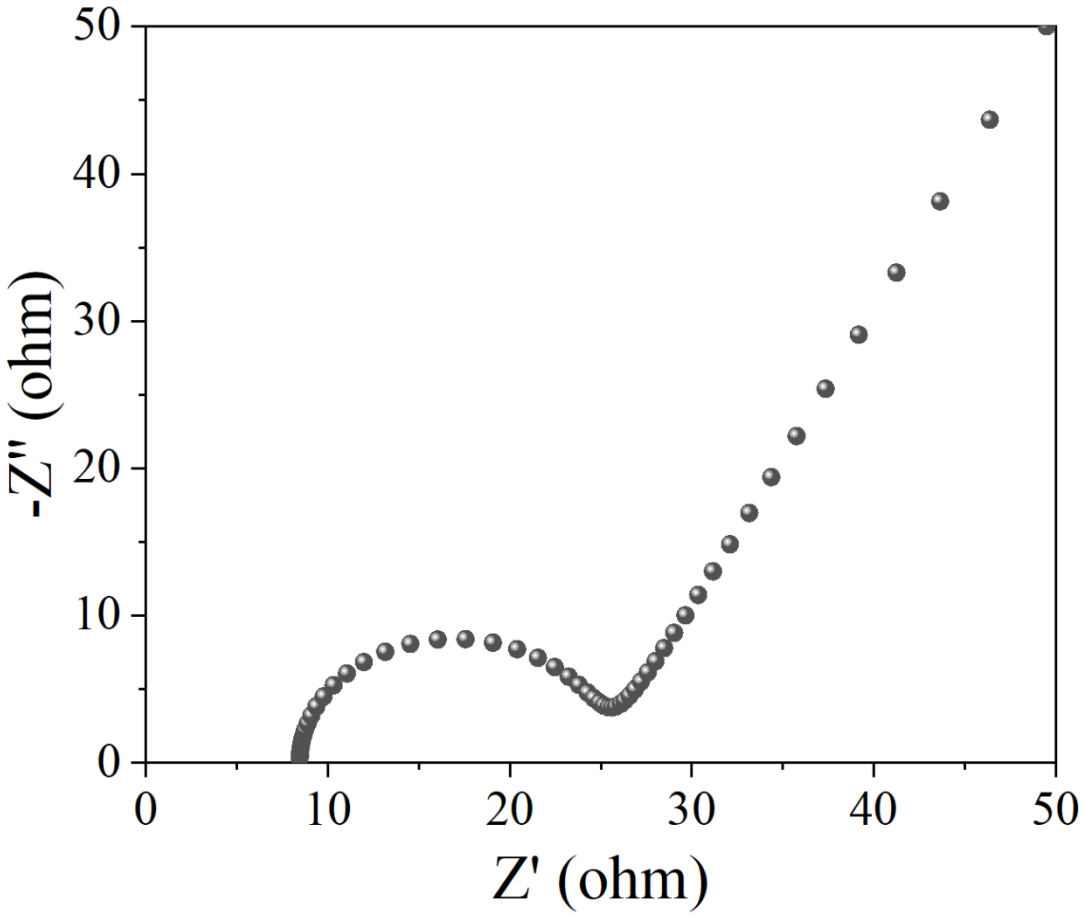

Figure S14. Nyquist plot of the CuS battery.